Journal of
Materials Chemistry A

Accepted Manuscript

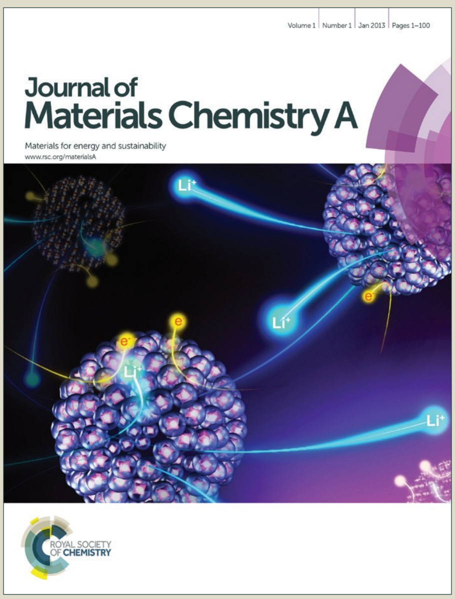

Journal Name

ARTICLE

# A Pure Organic Heterostructure of μ-oxo Dimeric Iron (III) Porphyrin and graphitic-$C_3N_4$ for Solar $H_2$ Production from Water

Received 00th January 20xx,
Accepted 00th January 20xx

DOI: 10.1039/x0xx00000x

www.rsc.org/

D. H. Wang, [ab] J. N. Pan, [ab] H. H. Li, [ab] J. J. Liu [ab] , Y. B. Wang, L. T. Kang*[ab] *and J. N. Yao**[c]

Due to the two-dimensional flexible structure and abundant pendant amine, graphitic-$C_3N_4$ (g-$C_3N_4$) may be easily modified by organic molecules as a promising photocatalyst for solar $H_2$ production from water. Here, through a simple liquid chemical reaction between g-$C_3N_4$ and the precursor of μ-oxo dimeric iron (III) porphyrin [$(FeTPP)_2O$], we provide a novel route to construct pure organic heterostructure of g-$C_3N_4$ / $(FeTPP)_2O$ on the basis of the π-π and the Fe−amine interactions. The experimental results demonstrated that $(FeTPP)_2O$ not just acted as a photosensitizer, but also played the role of charge promotor to prohibit the recombination of the excited electrons and holes for g-$C_3N_4$. As compared with pure or mixed g-$C_3N_4$ and/or $(FeTPP)_2O$, the obtained pure organic g-$C_3N_4$/$(FeTPP)_2O$ heterostructure exhibited a dramatic photocatalytic $H_2$ production under solar light without any cocatalysts.

## Introduction

The increasing worldwide energy shortage and environmental issues have stimulated intensive research on searching green technologies as sustainable ways to address these concerns. Among various potential solutions, solar $H_2$ production from water splitting offers an environmentally clean energy for the future and exhibits a method for solar energy storage and chemical energy conversion.[1-3] One ideal route for $H_2$ evolution is semiconductor-based water splitting under solar light irradiation.[4-7] The most challenging task in photocatalytic water splitting is to develop efficient and stable photocatalysts, which are capable of enough absorbing solar light for splitting water. At present, many semiconductors have been widely studied, mainly including inorganic materials such as metal oxides, metal sulfides and metal nitrides.[7-10]

G-$C_3N_4$, a new metal-free polymeric semiconductors,[11,12] stands out from a mass of photocatalysts as a shining star due to its appealing electronic structure with a medium band gap for both water reduction and oxidation, good chemical and physical stability.[13] Especially, the polymeric semiconductor is only composed of C and N elements, and can be easily prepared from low-cost and environmentally friendly precursors, [14-17] such as urea,[15] thiourea[16]and melamine[17,18]. The adjustable photocatalytic activity in visible light combing with its low cost make it potentially useful in a variety of applications.[19] The utilization of g-$C_3N_4$ as a photocatalyst for hydrogen evolution has been intensively studied in recent years, nevertheless, the photocatalytic efficiency of pristine g-$C_3N_4$ is still not satisfactory due to the rapid recombination of photo-excited electron-hole pairs, low visible utilization efficiency and small surface area.[20] To break these limitations, many strategy have been developed,[21-29] such as textural managing,[22-24] doping,[25,26] heterostructure construction[20,27] and dye sensitization[28,29] etc. Among them, the formation of heterostructures holds a great potential to separate the electron-hole pairs because it is helpful to the charge transfer across the interface of the heterostructure and restrains the recombination of electron and hole.[20,30] Now, semiconductor heterostructures are commonly applied in inorganic/inorganic and inorganic/organic semiconductors, but seldom observed in organic/organic system.[20,30-31] For organic semiconductors, Coulomb binding energies are observed in the range of several hundred meV for Frenkel exciton, which is higher as compared with that for Wannier exciton in inorganic semiconductors.[32,33] Thus, the fabrication and study of pure organic semiconductor heterostructures as photocatalysts , for example g-$C_3N_4$-P3HT polymer composite[34,35] and CNS-CN heterojunction[36], is very important in order to more efficiently avoid the rapid recombination of photo-generated hole and electron.

In fact, g-$C_3N_4$ may be easily modified with organic small molecules as a promising photocatalyst due to its two-dimensional flexible structure and abundant pendant amine. Here, $(FeTPP)_2O$ was chose to construct an pure organic heterostructure with g-$C_3N_4$ due to its strong absorption bands in visible region, large π-conjugated aromatic system and

[a.] Key Laboratory of design and assembly of functional nanostructures, Chinese Academy of Sciences, Fuzhou, 350002 (P.R. China).
E-mail: longtiank@fjirsm.ac.cn.
[b.] Fujian Provincial Key Laboratory of Nanomaterials, Fujian Institute of Research on the Structure of Matter, Chinese Academy of Sciences, Fuzhou, Fujian 350002 (P.R. China).
[c.] Beijing National Laboratory for Molecular Sciences (BNLMS), Institute of Chemistry, Chinese Academy of Sciences, Beijing 100190 ( P. R. China).
E-mail: jnyao@iccas.ac.cn.

Electronic Supplementary Information (ESI) available. See DOI: 10.1039/x0xx00000x outstanding chemical and thermal stability.[37] Furthermore, the $(FeTPP)_2O$ is found to be active centres in many enzymes, which has proven to be the versatile, potential catalysts for the oxidation of hydrocarbons in air in the absence of co-reductants or solvent.[38] Here, through a simple liquid chemical reaction between g-$C_3N_4$ and a precursor of $(FeTPP)_2O$, we provide a novel route to construct the heterostructure between g-$C_3N_4$ and organic small molecule on the basis of the π-π and the Fe–amine interactions. Unlike the similar reported several organic dye-sensitized $C_3N_4$ systems ,[39-41] in which they do not efficiently work without cocatalyst, $(FeTPP)_2O$ in our composite not only is photosensitizer for wider photon absorption, but also obviously promoted the separation of the photo-induced electrons and holes and the production of photocatalytic $H_2$ in the absence of cocatalyst**.**

## Results and discussions

The composite of g-$C_3N_4$/$(FeTPP)_2O$ was synthesized on the basis of the reduction of tetraphenyl iron (III) porphyrin perchlorate with g-$C_3N_4$ dispersion (see experimental section). In order to prove the existence of $(FeTPP)_2O$ in as-obtained samples, firstly, a sample was dissolved in dichloromethane ($CH_2Cl_2$) to obtain a yellow-green solution via filtration. Then, the UV-vis absorption spectrum and MALDI-TOF Mass Spectrometry (MS) were used to measure the solution, and the results were shown in Fig. S1. The UV-vis absorption spectrum in Fig. S1a shows three major absorption bands with $\lambda_{max}$ values at 407 nm (Soret band), 570 nm (Q-band) and 611 nm (Q-band), which belong to typical μ-oxo dimeric iron (III) porphyrin [$(FeTPP)_2O$].[38] The MS of the solution in Fig. S1B exhibits the existence of the ion of $(FeTPP)^+$, which is from ionic fragment of $(FeTPP)_2O$. In addition, pure $(FeTPP)_2O$ was also prepared by replacing $C_3N_4$ dispersion with pure water. The presence of the typical stretching mode of Fe–O–Fe at 870 and 895 $cm^{-1}$ further prove the dimeric μ-oxo iron(III) porphyrin structure,[38] as shown in Fig. S2.

The Fourier transform infrared spectroscopy (FTIR) spectra of pristine g-$C_3N_4$, pure $(FeTPP)_2O$ and a series of g-$C_3N_4$/$(FeTPP)_2O$ composites are obtained and shown in Fig. S3. For the pristine g-$C_3N_4$, the intense band at 812.1 $cm^{-1}$ represents the out-of-plane bending vibration characteristic of heptazine rings. The bands from 1000-1750 $cm^{-1}$ are from the stretching and bending modes of nitrogen containing heterocycles. The broad feature at 3250 $cm^{-1}$ is usually assigned to the stretching modes of -NH- groups.[42,43] Unfortunately, FTIR spectra in Fig. S3 exhibits the typical bands of g-$C_3N_4$, however no noticeable trace of $(FeTPP)_2O$ can be found on account of the low loading amount of $(FeTPP)_2O$ (lower than 10 wt%). Based on the above experimental results and analysis, the existence of $(FeTPP)_2O$ and g-$C_3N_4$ in as-obtained samples were proved, which indicates the successful synthesis of the composite of g-$C_3N_4$/$(FeTPP)_2O$ in this work.

To clarify whether the heterostructure is successfully formed in the composite of g-$C_3N_4$/$(FeTPP)_2O$, the optical properties of the above mentioned materials were studied. Fig. 1a shows the UV–vis diffuse reflectance spectroscopy (DRS) of g-$C_3N_4$/$(FeTPP)_2O$ composites, pure g-$C_3N_4$ and $(FeTPP)_2O$. The absorption peak of sole g-$C_3N_4$ is up to ~ 450 nm, and has a small absorption tail which is probably due to n-π* transitions.[44] The $(FeTPP)_2O$ has strong absorption in visible region from 400 to 700 nm, manly including two Q bands around 567 nm and 613 nm, which are similar to that of $(FeTPP)_2O$ solution (Fig. S1). The g-$C_3N_4$/$(FeTPP)_2O$ composites show the absorption features combining g-$C_3N_4$ and $(FeTPP)_2O$, and exhibit wider absorption of solar light. As the content of g-$C_3N_4$ increased, the obvious red-shift of Q band of $(FeTPP)_2O$ in composites can be found, which suggests π–π stacking interactions between g-$C_3N_4$ and $(FeTPP)_2O$.[45,46]

Photoluminescence (PL) is an effective and commonly used method to investigate the electron transfer property of semiconductor materials.[45,46] Fig. 1b displays the PL spectra of g-$C_3N_4$, pure $(FeTPP)_2O$ and g-$C_3N_4$/$(FeTPP)_2O$ nanocomposites. Obviously, g-$C_3N_4$ has a strong and wide emission, in contrast, $(FeTPP)_2O$ has negligible PL signal response when excited wavelength is 400 nm. The emission intensity of g-$C_3N_4$ remarkably decreased after it was combined with $(FeTPP)_2O$. It means that the recombination of photo-excited holes and electrons of g-$C_3N_4$ is largely prohibited by $(FeTPP)_2O$ and that the charge transfer occurs in the composites. The big red shift of PL spectra of g-$C_3N_4$ in these composites also demonstrates the existence of interaction between g-$C_3N_4$ and $(FeTPP)_2O$. On the basis of the above optical properties, it was guessed that their heterojunctions have been successfully prepared and the charge transfer may occur between them.

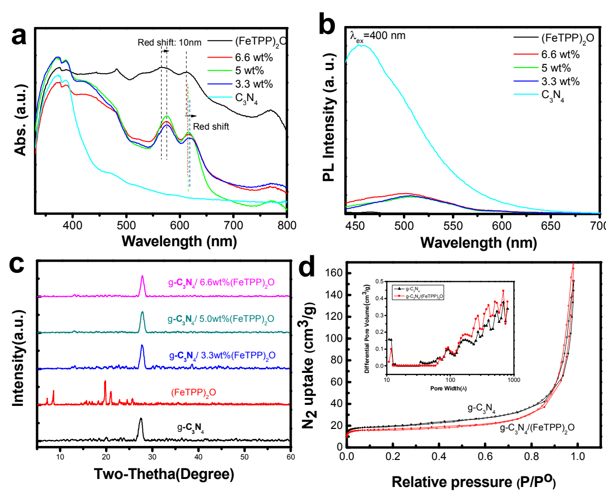


**Fig. 1** (a) UV–vis diffuse reflection spectra of g-$C_3N_4$, $(FeTPP)_2O$ and g-$C_3N_4$/$(FeTPP)_2O$ composites with different $(FeTPP)_2O$ content (3.3 wt%, 5 wt% and 6.6 wt%); (b) Photoluminescence spectra (excited at 400 nm) of g-$C_3N_4$, $(FeTPP)_2O$ and g-$C_3N_4$/$(FeTPP)_2O$ dispersion (1 mg/ml, water was used as the solvent), c )XRD patterns, d) Nitrogen adsorption-desorption isotherms with the corresponding pore size distribution curves (inset) for pure g-C3N4 and g-$C_3N_4$/$(FeTPP)_2O$ (5 wt%) .

Wide-angele X-ray diffraction (XRD) patterns also confirm the presence of g-$C_3N_4$ in as-prepared samples. As shown in Fig. 1c, XRD patterns of g-$C_3N_4$ with different $(FeTPP)_2O$ contents exhibit a typical diffraction peak at 27.41°, which is corresponding to interlayer stacking of aromatic segments and indexed as (002) . As compared with pure g-$C_3N_4$, no obvious $(FeTPP)_2O$ characteristic peaks can be found, indicating that g-$C_3N_4$/$(FeTPP)_2O$ keeps the original crystal structure of g-$C_3N_4$. The same conclusion can be also made from BET experiments. The nitrogen adsorption-desorption isotherms for pure g-$C_3N_4$ and $(FeTPP)_2O$-mediated g-$C_3N_4$ show type IV with hysteresis loops, indicating the presence of mesopores (Fig. 1d). The specific surface areas of pure g-$C_3N_4$ and g-$C_3N_4$/$(FeTPP)_2O$ (5.0 wt%) composites are 74 and 64 $cm^2/g$, respectively. Inserted image in Fig. 1d indicates the similar mesopores structure between pure g-$C_3N_4$ and g-$C_3N_4$/$(FeTPP)_2O$. These data suggest that the introduction of $(FeTPP)_2O$ into g-$C_3N_4$ lowers the specific surface areas of g-$C_3N_4$ , however does not have obvious effect on mesopores structure of g-$C_3N_4$, which is closely related with its photocatalytic activity.

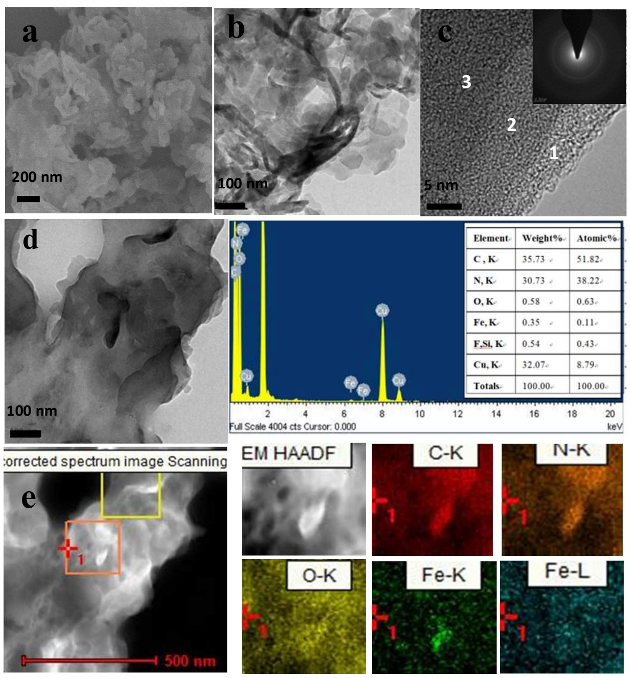


**Fig. 2** (a) SEM, (b) TEM, c) HRTEM images and SAED pattern, d) TEM images and corresponding EDS (Right), e) TEM images and corresponding mapping images (Right) of g-$C_3N_4$/$(FeTPP)_2O$ heterostructure including 5 wt% $(FeTPP)_2O$.

In order to further investigate the components and structure of g-$C_3N_4$/$(FeTPP)_2O$ composites, scanning electron microscopy (SEM, JSM-6700F, JEOL, Inc.) and transmission electron microscopy (TEM, F20, FEI) were used. The corresponding images were shown in Fig. 2. As compared with g-$C_3N_4$ shown in Fig. S4, which has smooth folded nanosheets of besides some fragments, $(FeTPP)_2O$ in Fig. S5 is composed of a lot of aggregations of amorphous nanoparticles (NPs) or naonoplates. After $(FeTPP)_2O$ was introduced into as-obtained g-$C_3N_4$, many small NPs can be found on g-$C_3N_4$ sheets and a quite of aggregations attach on g-$C_3N_4$, as shown in Fig. 2a and Fig. 2b. The TEM image in Fig. 2b exhibits that the g-$C_3N_4$/$(FeTPP)_2O$ heterostructure still keeps the morphology of g-$C_3N_4$. Fig. 2c clearly displays a typical layer-by-layer structure of g-$C_3N_4$ according to the difference of image contrast, and inserted selected area electric diffraction (SAED) image indicates a low crystallinity of g-$C_3N_4$ in the composite. A clue to the existence of $(FeTPP)_2O$ can be found in the TEM image shown in Fig. 2d. In order to further prove the existence of $(FeTPP)_2O$, the corresponding energy dispersive X-ray spectroscopy (EDS) was also performed on the sample. The result in Fig. 2d shows that Fe-K peaks exist in the spectrum and its percent content is calculated to be ~0.11 at.%, which is close to the content in theory (5 wt%). At same region of the sample, TEM-assisted elemental mappings were carried out and the results were shown in Fig.2e. Fe-K mapping in Fig. 2e further indicates that the NPs of $(FeTPP)_2O$ exist and they should be equably distributed on the surface of g-$C_3N_4$ nanosheets. The above results further demonstrate the successful formation of the g-$C_3N_4$/$(FeTPP)_2O$ heterostructure and the intimate contact between g-$C_3N_4$ and $(FeTPP)_2O$. Interestingly, although at least two obvious NPs can be found in orange square in Fig. 2e, as compared with Fig. 2d, only one $(FeTPP)_2O$ nanoparticle can be found in Fe-K mapping. It means that most of NPs or nanoplates should be fragments of g-$C_3N_4$ as a result of the reaction between g-$C_3N_4$ and precursor of $(FeTPP)_2O$.

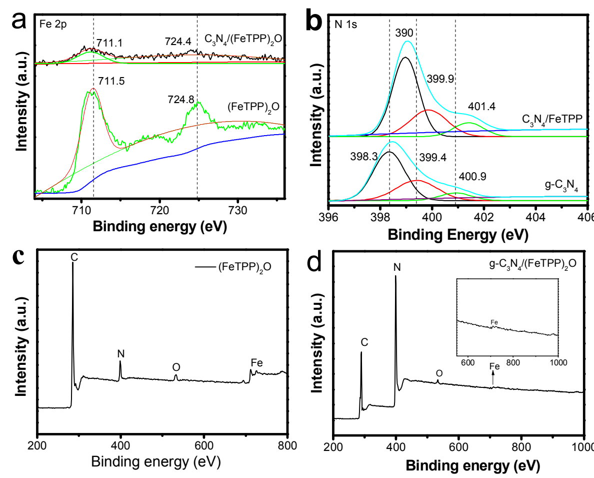


**Fig. 3** a) Fe 2p XPS spectra of pure $(FeTPP)_2O$ and g-$C_3N_4$/$(FeTPP)_2O$; b) N 1s XPS spectra of pure g-$C_3N_4$ and g-$C_3N_4$/$(FeTPP)_2O$ heterostructure.; c) and d) XPS spectra of pure $(FeTPP)_2O$ and g-$C_3N_4$/$(FeTPP)_2O$.

To further understand the interaction of the two components, X-Ray photoelectron spectroscopy (XPS) was performed on these samples. The binding energies of Fe $2p_{3/2}$ of $(FeTPP)_2O$ and g-$C_3N_4$/$(FeTPP)_2O$ are 711.5 ev and 711.1eV (Fig. 3a), respectively, the decrease of 0.4 eV in binding energy of Fe $2p_{3/2}$ might be caused by the interaction between $(FeTPP)_2O$ and g-$C_3N_4$, which indicates the formation of Fe-N bond because the N element has lower electron affinity than O.[47] The binding energy of Fe $2p_{1/2}$ also has the same tendency. To prove the interaction, N1s XPS of pure g-$C_3N_4$ and g-$C_3N_4$/$(FeTPP)_2O$ was also measured and compared, the results are exhibited in Fig. 3b. Three peaks at ca. 398.3, 399.4 and 400.9 eV are observed for single g-$C_3N_4$. The main N 1s peak at

398.3 eV corresponds to $sp^2$ hybridized aromatic N bonded to carbon atoms (C-N-C). The peak at 399.4 eV is assigned to the tertiary N bonded to carbon atoms in the form of N-(C)3 or H-N-(C)2. And the weak peak with high binding energy at 400.9 eV is attributed to quaternary N bonded three carbon atoms in the aromatic cycles.[15,42,43] After forming heterostructure with $(FeTPP)_2O$, all the N 1s peaks of g-$C_3N_4$ shift to higher binding energy, corresponding to the decrease of Fe 2p binding energy. Apparently, a strong interaction between $(FeTPP)_2O$ and g-$C_3N_4$ is built through the formation of Fe–N bond.[48] As compared with the relative atomic concentration of Fe (1.29 at%) in the pure $(FeTPP)_2O$ composite shown in Fig. 3c, that of g-$C_3N_4$/$(FeTPP)_2O$ composite is 0.21 atom% estimated from the XPS data. The result is higher than that from the EDS and our theoretical data because the XPS data are usually collected from the sample surface. The above XPS data indicate that in as-abstained samples, $(FeTPP)_2O$ is on the surface of g-$C_3N_4$ and they form heterostructure through π-π and the Fe–amine interactions.

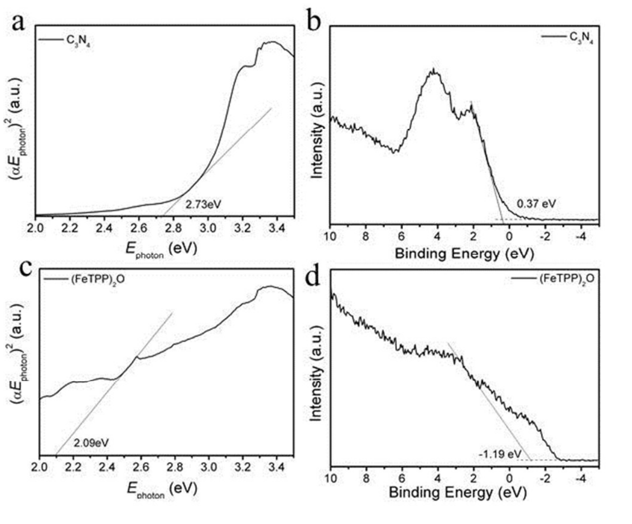


**Fig. 4** (a) Band-gap evaluation from the plots of $(\alpha E_{photon})^2$ *vs.* the energy of the absorbed light $E_{photon}$ for pristine g-$C_3N_4$; (b) VB XPS spectrum of pristine g-$C_3N_4$; (c) Band-gap evaluation from the plots of $(\alpha E_{photon})^2$ *vs.* the energy of the absorbed light $E_{photon}$ for pure $(FeTPP)_2O$; (d) VB XPS spectrum of pure $(FeTPP)_2O$.

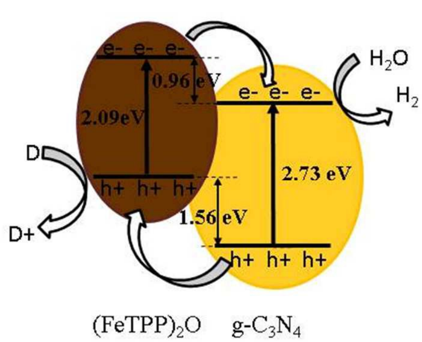


**Scheme 1.** The band-structure diagram of g-$C_3N_4$/$(FeTPP)_2O$ heterostructure.

Between g-$C_3N_4$ and $(FeTPP)_2O$, the charge transfer has been revealed in the PL spectra, the SEM, TEM and XPS data also have demonstrated the formation of the heterostructure. However, only the relative band positions of the two components can tell us the direction of charge transfer and the type of the heterojunction. Based on the UV–vis diffuse reflectance data, the band-gap energy was calculated according to Fig. 4a and Fig. 4c. The band gap of g-$C_3N_4$ and $(FeTPP)_2O$ are 2.73 eV and 2.09 eV, respectively. The valence band XPS (VB XPS) spectra of g-$C_3N_4$ and $(FeTPP)_2O$ were measured, as shown in Fig. 4b and Fig. 4d, the valence band (VB) of $(FeTPP)_2O$ is more negative about 1.56 eV than that of g-$C_3N_4$. Together with their band gaps we can deduce that the conduction band (CB) of $(FeTPP)_2O$ is more negative about 0.96 eV than that of g-$C_3N_4$. As illustrated in Scheme 1, the band alignment of g-$C_3N_4$ and $(FeTPP)_2O$ forms the typical type II heterojunction.[49,50] The large CB and VB offsets between g-$C_3N_4$ and $(FeTPP)_2O$ make the photo-generated electrons transfer from $(FeTPP)_2O$ to g-$C_3N_4$, while the photo-generated holes migrate from g-$C_3N_4$ to $(FeTPP)_2O$ in a thermodynamically favorable manner, which leads to an efficient charge separation and significant enhancement in photocatalytic activity.[36,50]

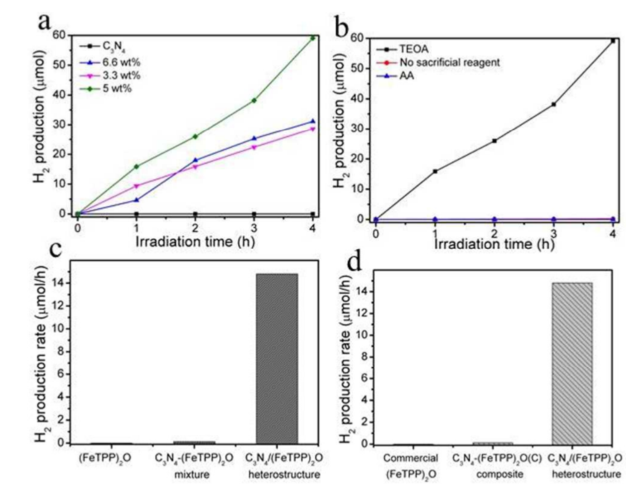


**Fig. 5** Under solar light, (a) time course of photocatalytic hydrogen evolution over g-$C_3N_4$, g-$C_3N_4$/$(FeTPP)_2O$ heterostructures with different contents of $(FeTPP)_2O$ (3.3 wt%, 5 wt% and 6.6 wt%); (b) Time course of photocatalytic hydrogen evolution over $C_3N_4$/$(FeTPP)_2O$ heterostructures (5 wt%) in the presence of various electron donors under solar light irradiation conditions; (c) Photocatalytic $H_2$ production rates over pure $(FeTPP)_2O$, g-$C_3N_4$ +$(FeTPP)_2O$ (5 wt%) mixture and g-$C_3N_4$/$(FeTPP)_2O$ (5 wt%) under solar light; (d) Photocatalytic $H_2$ production rates over commercial $(FeTPP)_2O$, g-$C_3N_4$/ commercial $(FeTPP)_2O$) mixture and g-$C_3N_4$/$(FeTPP)_2O$ heterostructure (5 wt%).

Solar-light-induced $H_2$ production was investigated to examine the photocatalytic activity of the as-prepared samples. Fig. 5a shows the varied amount of $H_2$ evolution under solar light for various photocatalysts. Almost no $H_2$ can be detected when only g-$C_3N_4$ was used as the photocatalyst. It may be due to the detrimental electron-holes recombination and the Frenkel exciton effect. In contrast, the g-$C_3N_4$/$(FeTPP)_2O$ composite exhibited dramatic photocatalytic $H_2$ production. Here, the loading amount of $(FeTPP)_2O$ plays an important role in tailoring the photocatalytic activity of the heterostructures.

With the content of $(FeTPP)_2O$ increased, the amount of $H_2$ first increases and then decreases. The experiments in Fig. 5 show that the optimal amount of $(FeTPP)_2O$ is about 5.0 wt%, and the best sample produces 59.2 μmol $H_2$ under solar light irradiation for 4h. As we know, for the photocatalytic activity of the heterostructure nanocomposites, two factors have serious effect on the hydrogen evolution. One is the capability of light absorption, the other is the amount of activity sites on the surface of composite. In our system, the $(FeTPP)_2O$ plays a dual roles of dye-sensitization and charge transfer for g-$C_3N_4$. In some ranges, more doping of guest means the formation of more heterojunctions (activity sites) and stronger absorption in visible-light. With the further increase of doping beyond some amount, however surface activity sites and/or absorption actually decrease. Therefore, there is always a optimal doping ratio. As far as g-$C_3N_4$/$(FeTPP)_2O$ composite is concerned, the decrease of its specific surface areas with the increasing of the amount of $(FeTPP)_2O$ (see Fig. 1d) means that the optimal ratio of $(FeTPP)_2O$ in the heterostructure is determined by its visible-light absorption. UV-vis DRS in Fig. 1a clearly shows that the ratio should be ~5.0 wt%, which is consistent with our experimental results in Fig. 5.

Furthermore, it was found that sacrificial electron donors are also essential for the consumption of photo-generated holes and the regeneration of $(FeTPP)_2O$. As shown in Fig. 5b, without any electron donors, no $H_2$ is produced. The presence of ascorbic acid (AA) also has little effect on promoting the activity of g-$C_3N_4$/$(FeTPP)_2O$ heterostructures, while the addition of triethanolamine (TEOA) significantly enhances the photocatalytic $H_2$ production. The reason must be ascribed to the highest redox potential and the created basic circumstance of TEOA.[51] Apparently, sole $(FeTPP)_2O$ shows no activity toward water splitting, as shown in Fig. 5c. It must be noted that the physical mixture of g-$C_3N_4$ and $(FeTPP)_2O$ failed to produce heterostructure, thus the mixture also shows negligible photocatalytic activity.[52] In addition, commercial $(FeTPP)_2O$ was also thought to combine with g-$C_3N_4$ in a physical manner. Through impregnating g-$C_3N_4$ with a dichlormethane solution of commercial $(FeTPP)_2O$ overnight, the composite of g-$C_3N_4$/$(FeTPP)_2O$ was prepared. However, Fig. 5d shows that the corresponding composite also exhibit negligible $H_2$ production. Therefore, the formation Fe-N bond between g-$C_3N_4$ and $(FeTPP)_2O$ should play a key role in the solar $H_2$ production from water splitting.

Hydrogen evolution measurement under UV-vis light irradiation with a 300 W Xeon lamp was also investigated. The durability of g-$C_3N_4$/$(FeTPP)_2O$ (5.0 wt%) acting as photocatalyst for $H_2$ evolution was evaluated by three consecutive operations. As shown in Fig. S6, UV-vis-light can stimulate the photocatalyst to produce $H_2$ at a rate of ~40 μmol/h and the amount of $H_2$ increases with irradiation time. Followed by the first run, some deactivation was observed in the second run. Interestingly, after the second cycle and lighting off for several hours, a little photocatalytic activity recovered in the third cycle. The deactivation should be happened by non-renewable consumption of the $(FeTPP)_2O$ in the photocatalytic process,[47] while the recovery is ascribed to the partial regeneration of $(FeTPP)_2O$ with TEOA in dark. In addition, under visible light ($\lambda$ > 420 nm) generated by Xeon lamp with a UV-cutoff filter, $H_2$ evolution is 11 μmol/h (see Fig. S7). At 420 nm, a quantum efficiency (QE) of 0.0415% was obtained.[53]

## Conclusions

In conclusion, through a simple liquid chemical reaction between g-$C_3N_4$ and the precursor of $(FeTPP)_2O$, we presented a novel route to construct pure organic heterostructure of g-$C_3N_4$ / $(FeTPP)_2O$ as a photocatalyst for solar $H_2$ production from water splitting. The $(FeTPP)_2O$ was found attaching on g-$C_3N_4$ through π–π interaction and Fe−N bond. The composite exhibited a significant enhancement in photocatalytic activity due to efficient light utilization and the charge separation which arises from the band offsets. Besides the loading amount of $(FeTPP)_2O$ and the type of sacrificial electron donors, it was found that the formation Fe−amine interactions between g-$C_3N_4$ and $(FeTPP)_2O$ should play a key role in the solar $H_2$ production from water splitting. Further study on the effect of Fe-N bond between g-$C_3N_4$ and $(FeTPP)_2O$ on photocatalytic activity is in progress. In a word, an efficient chemical path to significantly promote light harvesting and the charge transfer of g-$C_3N_4$ was achieved through constructing heterostructure between organic small molecule and g-$C_3N_4$. This work is expected to promote the research and application of g-$C_3N_4$ for solar $H_2$ production in the absence of cocatalyst.

## Experimental

**Materials.** Silver perchlorate, tetraphenyl iron (III) porphyrin chloride (FeTPPCl), anhydrous dichloromethane and acetonitrile (water < 30 ppm) were purchased from J&K Chemicals Co. Ultrapure water with a resistivity of 18.2 MΩ.cm was produced using Water Purifier apparatus (WP-UP-IV-20). Urea (10 g, AR) was obtained from Sinopharm Chemical Reagent Co., China.

**Synthesis of g-$C_3N_4$.** Graphitic carbon nitride (g-$C_3N_4$) was synthesized by thermal treatment of urea (10 g, AR) in a lidded high quality alumina crucible covered with aluminium foil under ambient pressure in air. The crucible was put in a high temperature box furnace (KSL-1100X-S) and heated to 600℃ for 3.0h, then raised to 650℃ for 0.5h to complete the reaction. The synthesized yellow mass was crushed to powder (330 mg) for further experiment.

**Synthesis of tetraphenyl iron (III) porphyrin perchlorate.** A precursor of tetraphenyl iron (III) porphyrin perchlorate was produced via reaction (1):

$$FeTPPCl + AgClO_4 = AgCl + FeTPP^{+}.ClO_4^{+} \quad (1)$$

In a typical synthesis, the solution of dry silver perchlorate in a minimum amount of anhydrous acetonitrile (0.6 mL, 0.30 mM) was added into a 16 mL solution of 0.27 mM FeTPPCl in anhydrous dichloromethane with stirring. After stirring for about 3h, the mixture was separated by centrifuging at 10,000 rpm for 10 min. Relying on the difference in solubility between silver chloride and $FeTPPClO_4$ in acetonitrile, brown $FeTPPClO_4$ solution is separated from the admixture. The solution was poured into 50 mL n-hexane and placed in fridge at -22℃ for 24h. Then the precipitation was obtained through centrifuging at 10,000 rpm for 2 min and further washed with n-hexane for two times. As-obtained product was dried for further using.

**Synthesis of $C_3N_4$/$(FeTPP)_2O$ (5wt%) nanocomposites.** Typically, g-$C_3N_4$ (80 mg) powder was added into 100 mL ultrapure water and sonicated at 800W for 2h. 4 mg of $FeTPPClO_4$ was dissolved in 8 mL anhydrous acetonitrile. Under stirring, the solution of $FeTPPClO_4$ was added dropwise into the $C_3N_4$ dispersion, and kept stirring for 1.5 h. The composite was obtained through vacuum filtration and washed twice with ultrapure water.

**Characterization.** FESEM images were recorded by a Hitach SU8010 instrument. Samples casted on copper grid were observed via transmission electron microscope (TEM, F20). The UV-Vis absorption spectra were obtained on a Perkin Elmer Lambda 950 UV-Vis spectrophotometer equipped with an integrating sphere. $BaSO_4$ was used as a reflectance standard in the diffuse reflectance experiments. FT-IR spectra were recorded on a VERTEX70 FTIR spectrometer when samples were embedded in KBr pellets. Photoluminescence (PL) spectra were recorded on a Hitachi F-4600 fluorescence spectrophotometer. X-Ray photoelectron spectroscopy (XPS) was performed with a Thermo Scientific ESCALAB 250Xi system. X-ray powder diffraction patterns were recorded by a Rigaku MiniFlex II diffractometer with a Cu sealed tube. $N_2$ physisorption isotherms of g-$C_3N_4$ and g-$C_3N_4$/$(FeTPP)_2O$ were measured by a Micromeritics ASAP 2020 surface area and porosimetry analyser.

**Photocatalytic activity measurements.** Photocatalytic water splitting reactions were carried out in a Pyrex top-irradiation reaction vessel connected to a glass closed gas circulation system (Labsolar III AG, Beijing Perfectlight Technology Co. Ltd). 80 mg $C_3N_4$, $C_3N_4$/$(FeTPP)_2O$ composites or 4 mg $(FeTPP)_2O$ was dispersed in 90 mL ultrapure water by sonication, and then 10 mL TEOA was added into. The reaction system was evacuated for 30 min to remove the dissolved gases in water prior to irradiation under a 300 W Xe lamp (PLS-SXE 300). A continuous magnetic stirrer was applied at the bottom of the reactor in order to keep the photocatalyst particles suspended in water during the whole experiment. The wavelength of the incident light was controlled by using a solar simulator filter for solar light irradiation. The temperature of the reactant solution was maintained at room temperature by a flow of cooling water during the reaction. The evolved gases were analyzed by gas chromatography (GC 7900, Shanghai Techcomp Instrument Ltd.). $H_2$ evolution under visible light ($\lambda$ > 420 nm) was measured by a 300 W Xe lamp combined with a UV-cutoff filter. The quantum efficiency (QE) was obtained by applying a Xe lamp (300 W) with a 420 nm bandpass filter. The number of incident photons was measured using a radiant power energy meter (MC UV-A). The QE was calculated using the following equation:

$$\mathrm{QE}(\%) = \frac{Number\ of\ reacted\ electrons}{Number\ of\ incident\ photons} \times 100\%$$

$$= \frac{2 * Velocity\ of\ H_2\ evolution\ (2k)}{Velocity\ of\ incident\ photons\ (q_p)} \times 100\%$$

## Acknowledgements

The authors gratefully acknowledge the financial from the National Natural Science Foundation of China (No. 21252001,21473204), the Special Project of National Major Scientific Equipment Development of China (No. 2012YQ120060), the Natural Science Foundation of Fujian Province (2015J01070), and Science and Technology Planning Project of Fujian Province, Grant No.2014H2008.

## Notes and references

1 A. J. Bard and M. A. Fox, *Acc. Chem. Res.*, 1995, **28**, 141.
2 S. S. Penner, *Energy*, 2006, **31**, 33; (c) A. J. Esswein and D. G. Nocera, *Chem. Rev.*, 2007, **107**, 4022.
3 K. Maeda and K. Domen, *J. Phys. Chem. Lett.*, 2010, **1**, 2655.
4 R. F. Service, *Science*, 2007, **315**, 789.
5 H. G. Kim, D. W. Hwang and J. S. Lee, *J. Am. Chem. Soc.*, 2004, **126**, 8912.
6 K. Maeda and K. Domen, *J. Phys. Chem. C*, 2007, **111**, 7851.
7 X. B. Chen, S. H. Shen, L. J. Guo and S. S. Mao, *Chem. Rev.*, 2010, **110**, 6503.
8 F. E. Osterloh, *Chem. Mater.*, 2008, **20**, 35.
9 K. Maeda, K. Domen, *Chem. Mater.* 2010, **22**, 612.
10 F. E. Osterloh, *Chem. Soc. Rev.*, 2013, **42**, 2294.
11 X. C. Wang, K. Maeda, A. Thomas, K. Takanabe, G. Xin, J. M. Carlsson, K. Domen and M. Antonietti, *Nat. Mater.*, 2009, **8**, 76.
12 S. W. Cao, J. X. Low , J. G. Yu and M. Jaroniec, *Adv. Mater.,* 2015, **27**, 2150.
13 Y. Zheng, J. Liu, J. Liang, M. Jaroniec and S. Z. Qiao, *Energy Environ. Sci.*, 2012, **5**, 6717.
14 A. Thomas, A. Fischer, F. Goettmann, M. Antonietti, J. O. Müller, R. Schlögl and J. M. Carlsson, *J. Mater. Chem.*, 2008, **18**, 4893.
15 F. Dong, L. W. Wu, Y. J. Sun, M. Fu, Z. B. Wu and S. C. Lee, *J. Mater. Chem.*, 2011, **21**, 15171.
16 Y. W. Zhang, J. H. Liu, G. Wu and W. Chen, *Nanoscale*, 2012, **4**, 5300.
17 H. J. Yan, Y. Chen and S. M. Xu, *Int. J. Hydrogen Energy*, 2012, **37**, 125.
18 Y. J. Zhong, Z. Q. Wang, J. Y. Feng, S. C. Yan, H. T. Zhang, Z. S. Li and Z. G. Zou, *Appl. Surf. Sci.,* 2014, **295**, 253.
19 Y. Wang, X. C. Wang and M. Antonietti, *Angew. Chem. Int. Ed.*, 2012, **51**, 68.
20 Z. W. Zhao, Y. J. Sun and F. Dong, *Nanoscale*, 2015, **7**, 15.
21 S. Cao and J. Yu, *J. Phys. Chem. Lett.*, 2014, **5**, 2101.
22 X. C. Wang, K. Maeda, X. F. Chen, K. Takanabe, K. Domen, Y. D. Hou, X. Z. Fu and M. Antonietti, *J. Am. Chem. Soc.*, 2009, **131**, 1680.

23 J. S. Zhang, M. W. Zhang, C. Yang and X. C. Wang, *Adv. Mater.*, 2014, **26**, 4121.
24 J. H. Sun, J. S. Zhang, M. W. Zhang, M. Antonietti, X. Z. Fu and X. C. Wang, *Nat. Commun.*, 2012, **3**, 1139.
25 Z. Z. Lin and X. C. Wang, *Angew. Chem. Int. Ed.*, 2013, **52**, 1735.
26 G. G. Zhang, M. W. Zhang, X. X. Ye, X. Q. Qiu, S. Lin and X. C. Wang, *Adv. Mater.*, 2014, **26**, 805.
27 L. Ge, F. Zuo, J. K. Liu, Q. Ma, C. Wang, D. Z. Sun, L. Bartels and P. Y. Feng, *J. Phys. Chem. C*, 2012, **116**, 13708.
28 Y. F. Zhang, F. Mao, H. J. Yan, K. W. Liu, H. M. Cao, J. G. Wu and D. Q. Xiao, *J. Mater. Chem. A,* 2015, **3**, 109.
29 X. H. Zhang, T. Y. Peng, L. J. Yu, R. J. Li, Q. Q. Li and Z. Li, *ACS Catal.*, 2015, **5**, 504.
30 H. L. Wang, L. S. Zhang, Z. G. Chen, J. Q. Hu, S. J. Li, Z. H. Wang, J. S. Liu and X. C. Wang, *Chem. Soc. Rev.*, 2014, **43**, 5234.
31 S. J. A. Moniz, S. A. Shevlin, D. J. Martin, Z. X. Guo and J. W. Tang, *Energy Environ. Sci.*, 2015, **8**, 731.
32 M. Muntwiler, Q. Yang, X. Zhu, *J. Electron Spectrosc. Relat. Phenom.*, 2009, **174**, 116.
33 C. Piliego and M. A. Loi, *J. Mater. Chem.*, 2012, **22**, 4141.
34 H. J. Yan and Y. Huang, *Chem. Commun.*, 2011, **47**, 4168.
35 X. J. Bai, C. P. Sun, S. L. Wu and Y. F. Zhu, *J. Mater. Chem. A,* 2015, **3**, 2741.
36 J. S. Zhang, M. W. Zhang, R. Q. Sun and X. C. Wang, *Angew. Chem.*, 2012, **124**, 10292.
37 T. Higashino and H. Imahori, *Dalton Trans.*, 2015, **44**, 448.
38 Q. Liu, Y. Z. Gong, C. J. Gong, Q. H. Li and C. C. Guo, *J. Porphyr. Phthalocya.*, 2009, **13**, 854.
39 K. Takanabe, K. Kamata, X. C. Wang, M. Antonietti, J. Kubota and K. Domen, *Phys. Chem. Chem. Phys.*, 2010, **12**, 13020.
40 J. Y. Xu, Y. X. Li, S. Q. Peng, G. X. Lu and S. B. Li, *Phys. Chem. Chem. Phys.*, 2013, **15**, 7657.
41 L. J. Yu, X. H. Zhang, C. S. Zhuang, L. Lin, R. J. Li and T. Y. Peng, *Phys. Chem. Chem. Phys.*, 2014, **16**, 4106.
42 J. H. Liu, T. K. Zhang, Z. C. Wang, G. Dawson and W. Chen, *J. Mater. Chem.*, 2011, **21**, 14398.
43 D. J. Martin, K. P. Qiu, S. A. Shevlin, A. D. Handoko, X. W. Chen, Z. X. Guo and J. W. Tang, *Angew. Chem. Int. Ed.*, 2014, **53**, 9240.
44 A. B. Jorge, D. J. Martin, M. T. S. Dhanoa, A. S. Rahman, N. Makwana, J. W. Tang, A. Sella, F. Corà, S. Firth, J. A. Darr and P. F. McMillan, *J. Phys. Chem. C*, 2013, **117**, 7178.
45 D. M. Chen, K. W. Wang, W. Z. Hong, R. L. Zong, W. Q. Yao and Y. F. Zhu, *Appl. Catal. B: Environ.*, 2015, **166**, 366.
46 M. S. Zhu, Z. Li, B. Xiao, Y. T. Lu, Y. K. Du, P. Yang and X. M. Wang, *ACS Appl. Mater. Inter.*, 2013, **5**, 1732.
47 D. D., Wang, J. Huang, X. Li, P. Yang, Y. K. Du, C. M. Goh and C. Lu, *J. Mater. Chem. A*, 2015, **3**, 4195.
48 D. H. Wang, L. Jia, X. L. Wu, L. Q. Lu and A. W. Xu, *Nanoscale*, 2012, **4**, 576.
49 S. S. Chen, Y. Qi, T. Hisatomi, Q. Ding, T. Asai, Z. Li, S. S. K. Ma, F. X. Zhang, K. Domen and C. Li, *Angew. Chem. Int. Ed.*, DOI: 10.1002/anie.201502686.
50 M. R. Gholipour, C. T. Dinh, F. Bélandb and T. O. Do, *Nanoscale*, 2015, **7**, 8187.
51 X. H. Zhang, L. J. Yu, C. S. Zhuang, T. Y. Peng, R. J. Li and X. G. Li, *ACS Catal.*, 2014, **4**, 162.
52 S. W. Cao, Y. P. Yuan, J. Barber, S. C. J. Loo and C. Xue, *Appl. Surf. Sci.,* 2014, **319**, 344.
53 The measurement of quantum efficiency at 420 nm: $k=1.01*10^{-9}$ mol/s, k is numbers of $H_2$ evolution per second. $q_p=p*\lambda/(h*c)$, in which $q_p$ is the number of photons per second, P is illumination intensity (1.387J/s), λ is incident wavelength of 420 nm, c is the speed of light ($3*10^8$ m/s), h is Planck's constant ($6.626*10^{-34}$ J/s). Thus, $QE=2k/q_p=(2*1.01*10^{-9}$ mol/s)/($4.87*10^{-6}$ mol/s) = 0.0415 %.

Table of Content:

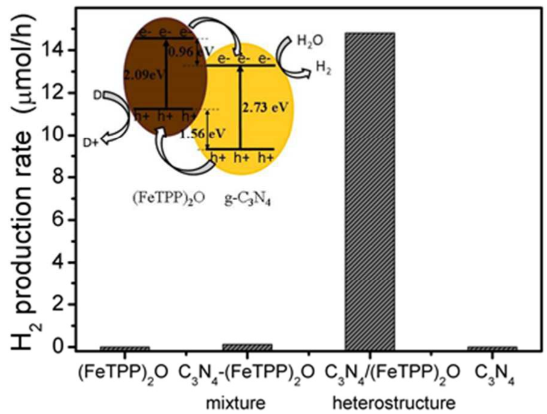


A novel pure organic heterostructure was constructed between g-$C_3N_4$ and $(FeTPP)_2O$ as a photocatalyst for solar $H_2$ production from water splitting.